

Featuring work in optofluidics and biosensors from the VALENS Centre for Bio Devices and Signal Analysis in the School of Electrical and Electronic Engineering at Nanyang Technological University of Singapore.

Title: Cell refractive index for cell biology and disease diagnosis: *past, present and future*

We review cell refractive index models and measurement techniques for the last 50 years. The applications and significance of cell refractive index in cell biology, hematology, pathology, and the future research trends in the field are discussed.

### As featured in:



See L. K. Chin, W. Ser, Y. Leprince-Wang et al. *Lab Chip*, 2016, 16, 634.



[www.rsc.org/loc](http://www.rsc.org/loc)

Registered charity number: 207890



Cite this: *Lab Chip*, 2016, 16, 634

## Cell refractive index for cell biology and disease diagnosis: *past, present and future*

P. Y. Liu,<sup>ab</sup> L. K. Chin,<sup>\*b</sup> W. Ser,<sup>\*b</sup> H. F. Chen,<sup>b</sup> C.-M. Hsieh,<sup>b</sup> C.-H. Lee,<sup>c</sup> K.-B. Sung,<sup>d</sup> T. C. Ayi,<sup>e</sup> P. H. Yap,<sup>f</sup> B. Liedberg,<sup>g</sup> K. Wang,<sup>hi</sup> T. Bourouina<sup>j</sup> and Y. Leprince-Wang<sup>\*a</sup>

Cell refractive index is a key biophysical parameter, which has been extensively studied. It is correlated with other cell biophysical properties including mechanical, electrical and optical properties, and not only represents the intracellular mass and concentration of a cell, but also provides important insight for various biological models. Measurement techniques developed earlier only measure the effective refractive index of a cell or a cell suspension, providing only limited information on cell refractive index and hence hindering its in-depth analysis and correlation. Recently, the emergence of microfluidic, photonic and imaging technologies has enabled the manipulation of a single cell and the 3D refractive index of a single cell down to sub-micron resolution, providing powerful tools to study cells based on refractive index. In this review, we provide an overview of cell refractive index models and measurement techniques including microfluidic chip-based techniques for the last 50 years, present the applications and significance of cell refractive index in cell biology, hematology, and pathology, and discuss future research trends in the field, including 3D imaging methods, integration with microfluidics and potential applications in new and breakthrough research areas.

Received 26th November 2015,  
Accepted 16th December 2015

DOI: 10.1039/c5lc01445j

www.rsc.org/loc

## Introduction

Cell biophysics uses physical models and theories to study cells, such as the mechanical, electrical and optical properties of cells. Mechanical parameters such as elasticity, adhesive force and speed are studied to analyze how cells respond to forces or migrate by deformation, *etc.*<sup>1</sup> Electrical parameters such as conductivity, impedance and electromotive force are important for studies of neural networks such as the propagation of electrical synapses.<sup>2</sup> Similarly, optical parameters such as adsorption, scattering, reflection, *etc.* determine how light propagates in a cell, and these optical parameters are strongly correlated with intracellular mass and concentration.<sup>3,4</sup> One

of the most important biophysical properties is the refractive index of a single cell, which has been studied and measured since the 1950s. It can be used to determine or correlate with other cell biophysical parameters (such as dry mass, wet mass, protein concentration, elasticity, conductivity, *etc.*), and to study certain cell metabolic activities (such as cell division, infection, *etc.*). In fact, cell refractive index is not a stranger to life scientists. In flow cytometry, forward and side scattering intensities are often measured whereby the side scattering intensity is related to the cell refractive index. Optical density is used to correlate with bacteria concentration, which is also dependent on the refractive index of bacteria.

Several models of cell refractive index have been developed in the last 50 years based on different measurement techniques, which include (1) the average refractive index of a cell population suspended in a medium; (2) the effective refractive index of a single cell; and (3) the 2D and 3D refractive indices of a single cell. The effective refractive index of a single cell is more precise as compared to the average refractive index of a cell population. However, both models are limited in providing sufficient information for biological applications with only a single refractive index value to represent a cell. More sophisticated and complex optical systems are developed to measure the 2D refractive index profile in a surface layer and, more recently, the 3D refractive index profile of a single cell. Both models provide more in-depth refractive index information down to sub-micron resolution. With this in-depth refractive index information,

<sup>a</sup> Université Paris-Est, UPEM, F-77454 Marne-la-Vallée, France.

E-mail: yamin.leprince@u-pem.fr

<sup>b</sup> School of Electrical and Electronic Engineering, Nanyang Technological University, 639798 Singapore. E-mail: lkchin@ntu.edu.sg, ewser@ntu.edu.sg

<sup>c</sup> Research Center for Applied Sciences, Academia Sinica, Taipei 11529, Taiwan

<sup>d</sup> Department of Electrical Engineering, National Taiwan University, Taipei 106, Taiwan

<sup>e</sup> Defence Medical & Environmental Institute, DSO National Laboratories, 117510 Singapore

<sup>f</sup> Lee Kong Chian School of Medicine, Nanyang Technological University, 308232 Singapore

<sup>g</sup> Interdisciplinary Graduate School, Nanyang Technological University, 639798 Singapore

<sup>h</sup> Institute of Biology Chemistry, Academia Sinica, Taipei 115, Taiwan

<sup>i</sup> College of Medical Science and Technology, Taipei Medical University, Taipei 110, Taiwan

<sup>j</sup> Université Paris-Est, ESYCOM, ESIEE, F-93162 Marne-la-Vallée, Paris, France



biologists and biomedical researchers can use cell refractive index to study a single cell or a group of cells for the applications of cell biology and disease diagnosis, attempting to obtain biological insight into the research of biophysics.

To date, several cell refractometers have demonstrated the synergy of microfluidics with optical imaging systems, which provide several benefits including (1) manipulating and mixing liquids with high flexibility and stability for cell behavior analysis, long-term cell culture, *etc.*, (2) manipulating and trapping cells or even bacteria with high controllability and specificity for single or group cell analysis, and (3) high biocompatibility in terms of materials and biochemical processes that enable living cell analysis. Microfluidics with robust cell manipulation techniques and highly controllable culture conditions can facilitate non-contact refractive index measurement and mapping with high precision or even for long-term refractive index monitoring.

In this review, we provide an overview of cell refractive index models, starting from the average cell refractive index of suspended cells and the effective refractive index of a single cell to 2D and 3D refractive indices of a single cell, and their respective measurement techniques including microfluidic chip-based techniques. Next, we review the biological insights provided by the cell refractive index for various applications such as cell morphology and growth in cell biology, malaria and anemia disease diagnosis in hematology, and cancer cell and circulating tumor cell detection in pathology. Finally, we discuss the outlook, research trends and applications of cell refractive index, including 3D imaging methods, integration with microfluidics and its potential applications in new and breakthrough research areas.

### Cell refractive index models and their measurements

The simplest model of cell refractive index measurement is the average refractive index of cells suspended in a medium

(Fig. 1a). Suspended cells are assumed to be homogeneous with the same refractive index and the average cell refractive index can be determined by measuring either the refractive index change using interference refractometry or the optical density using optical densitometry.<sup>5</sup> For interference refractometry, the average refractive index of suspended cells ( $n_{\text{cell}}$ ) can be determined based on the classical mixture equation as

$$n_{\text{cell}} = n_{\text{medium}} + \frac{\Delta n}{V_{\text{cell}}}, \text{ where } n_{\text{medium}} \text{ is the refractive index of the}$$

medium,  $V_{\text{cell}}$  is the volume fraction of cells in the medium and  $\Delta n$  is the refractive index difference measured by interference refractometry. On the other hand, in optical densitometry, the refractive index of the medium is changed incrementally and the optical density is measured. Maximum transmission occurs when the refractive index of the medium and that of the suspended cells match. Other methods based on light scattering and transmission were demonstrated.<sup>6,7</sup> The main drawback of this model is its simplicity without any in-depth refractive index information provided. The large variation of cell refractive index within the same cell type cannot be measured and analyzed.

In 1953, R. Barer proposed a more detailed refractive index model based on a single cell.<sup>8</sup> Since a cell is mainly composed of cytoplasm and proteins occupy the greatest portion of cell solids in the cytoplasm, a single cell is treated as a container filled with a protein solution (Fig. 1b). Effective cell refractive index is defined as  $n_{\text{cell}} = n_o + \alpha C$ , where  $n_o$  is the refractive index of water or dilute salt solution,  $\alpha$  is the specific refraction increment and  $C$  is the mass density of protein in gram per deciliter ( $\text{g dL}^{-1}$ ).<sup>9,10</sup> Based on this model, the effective cell refractive index is linearly proportional to the concentration of protein in the cell. Several unconjugated proteins were measured and the specific refraction increment for proteins is found to be  $1.845 \times 10^{-3} \pm 0.037 \times 10^{-3}$ .<sup>9</sup> Therefore, the refractive index of a protein solution increases by

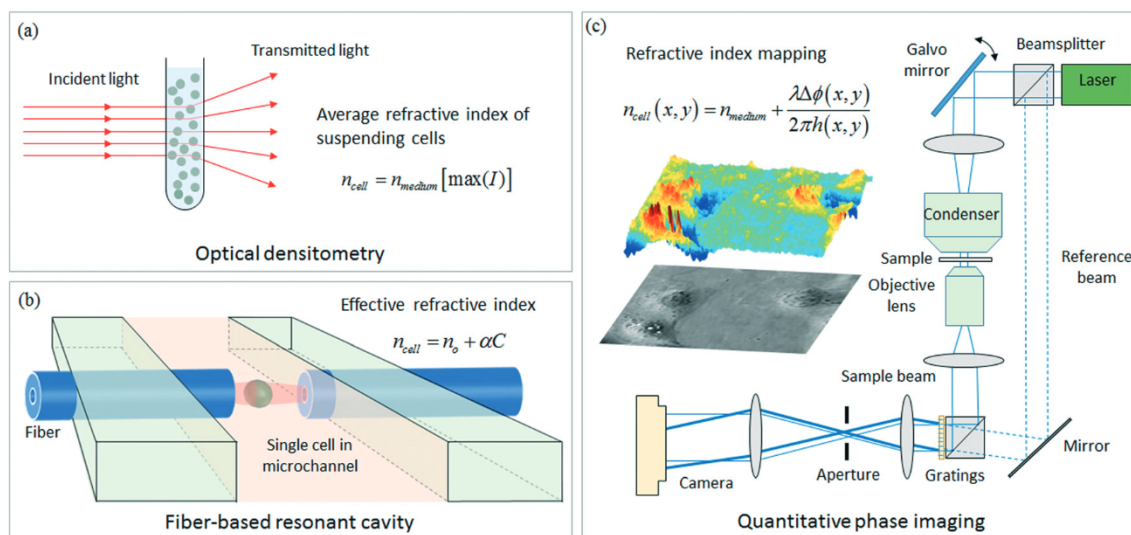


**Fig. 1** Cell refractive index models: (a) average refractive index of cells suspended in a medium measured by optical densitometry, (b) effective refractive index of a single cell measured by resonant cavity, and (c) refractive index mapping measured by quantitative phase microscopy.

$1.845 \times 10^{-3}$  for every one percent increase in the concentration. Most research reports indicate that the refractive index of the protein solution is linear to the concentration of the protein. Barer showed that indeed the variation of refractive index as the protein concentration increases is a linear relationship with an insignificant discrepancy even at high protein concentrations. Although lipids and carbohydrates exist in the cytoplasm, they occur as complexes, which have similar refraction increments to proteins. The influence of pH on the specific refraction increment was investigated and the results showed that the effect of pH is small and negligible.<sup>10</sup> Similarly, the effects of temperature and salt concentration were investigated and their effects on the specific refraction increment were small and within 0.5% to 2%.<sup>10</sup>

Several different methods have been developed to measure the effective refractive index of a single cell. Immersion refractometry exploits the intensity contrast between a cell and its surrounding medium using phase contrast microscopy whereby the cell appears invisible when its effective refractive index matches with that of the surrounding medium.<sup>11</sup> A similar method integrated into a microfluidic chip was demonstrated to measure the effective refractive index of a single bacterium that is trapped in a microfluidic channel.<sup>12</sup> In addition, several microfluidic chips integrated with various optical techniques were demonstrated to measure the effective refractive index, dry mass and water mass of a single living cell, such as light scattering,<sup>13</sup> laser resonant cavity,<sup>14</sup> FP resonant cavity,<sup>15</sup> grating resonant cavity with optical trap,<sup>16</sup> Mach-Zehnder interferometer,<sup>17</sup> etc. A resolution up to  $10^{-3}$  refractive index unit (RIU) was demonstrated.<sup>16</sup> Most of these techniques measure the optical path difference caused by the cell in the medium and decouple its effective refractive index and size by a differential buffer method.<sup>15–17</sup> The main drawback of these techniques is the assumption of a single living cell as a spherical object filled with a protein solution. In reality, cells exist in different shapes and other organelles exist in the cell especially cell nucleolus that is denser than the cytoplasm. In most cases, minor changes in the concentration and the abundance of various intracellular organelles are not reflected in the effective refractive index. Therefore, the study of effective refractive index does not provide many details to understand sophisticated cell biological processes.

With the recent development in advanced optical imaging systems, the 2D and 3D refractive indices of a single cell down to the sub-micron resolution are now feasible and demonstrated (Fig. 1c). A cell is no longer treated as a homogeneous entity filled with a protein solution, but an entity with a spatial refractive index distribution. Localized surface plasmon excitation by using a near-field probe was developed to obtain the 2D refractive index of cell samples on a focal plane by scanning point-by-point.<sup>18,19</sup> A spatial resolution of several tenths of nanometers with a resolution of  $10^{-5}$  RIU was demonstrated.<sup>19</sup> However, it is time consuming since scanning point-by-point is required. One new trend for cell refractive index mapping is quantitative phase imaging.<sup>20–29</sup> The phase delay map ( $\Delta\phi$ ) that is diffracted by the cell

consists of the structural and optical information of the cell,

i.e.  $n_{\text{cell}}(x, y) = n_{\text{medium}} + \frac{\Delta\phi(x, y)\lambda}{2\pi h_{\text{cell}}(x, y)}$ , where  $x$  and  $y$  are the

spatial coordinates,  $\lambda$  is the wavelength of light and  $h_{\text{cell}}(x, y)$  is the cell thickness. Since the cell refractive index is linearly proportional to the protein concentration, the dry mass density of the cellular matter can be determined as

$\sigma(x, y) = \frac{\lambda}{2\pi\alpha} \Delta\phi(x, y)$ , where  $\alpha$  is the specific refraction

increment in  $\text{ml g}^{-1}$ . One of the quantitative phase imaging techniques is based on the off-axis configuration whereby the reference and sample beams are deviated with a small angle difference, which include digital holographic microscopy<sup>21,22</sup> and Hilbert phase microscopy.<sup>23</sup> The interference image of the cell, resulting from the overlap of the reference and sample beams, is captured and the phase map can be extracted from the interference image through phase unwrapping and background subtraction algorithms. By knowing and making assumption on the shape of the cell, the 2D refractive index profile can be obtained. The demonstrated refractive index resolution was as low as  $10^{-4}$  RIU.<sup>22</sup> Another technique is based on the phase-shifting method whereby four phase-shifted interference images ( $\pi/2$  per frame) are captured and phase maps are extracted from the interference image through a phase unwrapping algorithm.<sup>24,25</sup> Although the off-axis method is fast with a single image, the phase-shifting method maintains a diffraction-limited transverse resolution (250 nm). For higher stability down to mrad levels, a common-path configuration is demonstrated whereby a diffraction grating is used to create a reference beam that travels through the same optical path as the sample beam.<sup>26</sup> For the 3D refractive index measurement of a single cell, a series of phase images are captured at various angles and the 3D refractive index profile can be reconstructed by algorithms such as filtered back-projection or optical diffraction tomography.<sup>27,28</sup> Recently, the 3D refractive index measurement of a single cell flowing in a microfluidic channel has been demonstrated.<sup>29</sup> In such a system, a series of angular spectra are generated when the cell passes through a line-focused beam (sample beam of Mach-Zehnder interferometry) via microfluidics. Similarly, the 3D refractive index of the cell can be reconstructed. The achieved specifications of various measurement techniques including the tomographic bright-field imaging technique<sup>30</sup> are summarized in Table 1.

### Biological insight and applications

With the capability to measure the refractive index of a single cell, the representative position of refractive index in cell biology has been widely studied. Initially, researchers measured the refractive index of different biological samples ranging from tissues and cells to bacteria and viruses. Subsequently, the refractive index of normal cells and abnormal cells was measured and compared to search for the correlation with



**Table 1** Cell refractive index models and various measurement techniques

Cell refractive index model	Measurement technique	Refractive index resolution (RIU)	Minimal mass density change (pg fl <sup>-1</sup> )*	Spatial resolution (nm)	Ref.
Average refractive index of suspended cells	Interference refractometer	$3 \times 10^{-3}$	0.0163	—	5
	Optical densitometer	$3 \times 10^{-3}$	0.0163	—	5
	Light scattering	$10^{-2}$	0.0542	—	6
	Light transmission and reflection	$10^{-2}$	0.0542	—	7
Effective refractive index of a single cell	Immersion refractometer	$1 \times 10^{-3}$	0.0054	—	11, 12
	Light scattering	$1 \times 10^{-2}$	0.0542	—	13
	Laser resonant cavity	$4 \times 10^{-3}$	0.0217	—	14
	FP resonant cavity	$3 \times 10^{-3}$	0.0163	—	15
	Grating resonant cavity	$1 \times 10^{-3}$	0.0054	—	16
	Mach-Zehnder interferometer	$1 \times 10^{-3}$	0.0054	—	17
Refractive index mapping	Surface plasmon nano-optical probe	$4 \times 10^{-5}$	0.0002	80	18, 19
	Confocal quantitative phase microscopy	$4 \times 10^{-3}$	0.0217	—	20
	Digital holographic microscopy	$1 \times 10^{-2}$	0.0542	—	21
		$3 \times 10^{-4}$	0.0016	—	22
	Hilbert phase microscopy	$2 \times 10^{-3}$	0.0108	1000	23
	Phase-shifting interferometry	$9 \times 10^{-3}$	0.0488	250	24
		$3 \times 10^{-4}$	0.0016	—	25
	Common-path tomographic diffractive microscopy	$1 \times 10^{-3}$	0.0054	—	26
	Microfluidic off-axis holography	$5 \times 10^{-3}$	0.0271	350	29
	Tomographic bright-field imaging	$8 \times 10^{-3}$	0.0434	260	30

\* $\alpha = 0.1845 \text{ ml g}^{-1}$  is used to calculate the minimal mass density change to be detected by the respective measurement techniques.

diseases such as cancer, malaria, anemia, bacterial infection, *etc.* In this section, the applications of refractive index in three different research fields are discussed. They are cell biology, hematology and pathology.

**Cell biology.** The effective refractive index of various cells has been widely demonstrated and due to many advances in methodology and measurement systems, we are now able to measure the refractive indices of various components of the cell such as cytoplasm and nucleus. For example, live HeLa cells suspended in culture medium were measured by using tomographic phase imaging and the refractive index of the nucleus is between 1.355–1.365 RIU, while the refractive index of the cytoplasm is 1.360–1.390 RIU and the nucleoli have the highest refractive index at 1.375–1.385 RIU.<sup>28</sup> Typical refractive index values of various organelles are shown in Table 2. These results provide new insight into cell biology because, previously, it is widely claimed that the refractive index of nucleus is higher than that of cytoplasm.<sup>33</sup> Similar results are obtained with other cell lines such as HEK 293 cells whereby small cytoplasmic particles (possibly lipid droplets, vacuoles or other organelles) with high refractive indices are observed.

**Table 2** Typical refractive index values for various organelles in a cell

Organelles/intracellular matter	Refractive index	References
Cytosol	1.360–1.390	28
Nucleus	1.355–1.365	28
Nucleolus	1.375–1.385	28
Mitochondria	1.400–1.420	31
Lysosome	1.600	32

The refractive index of various bacteria has also been widely measured and studied throughout the years. Based on suspension techniques, *E. coli* was measured with an average refractive index of 1.401 and 1.406 RIU by using interference refractometry and optical densitometry, respectively.<sup>5</sup> The measured average refractive index of a suspended *E. coli* is relatively higher than the measured effective refractive index of a single *E. coli*. With immersion refractometry, the effective refractive index of *E. coli* was measured to be 1.386 RIU.<sup>12</sup> The basic model of a single *E. coli* was studied whereby the nucleoid, which is clearly visible under a phase-contrast microscope, is separated from the cytoplasm. The contrast between the nucleoid and the cytoplasm resulted from the difference in refractive index and solid concentration. The cytoplasm with RNA (0.5% wt/vol) and protein (21% wt/vol) has a refractive index of 1.390 RIU, while the nucleoid mainly with DNA (6.8% wt/vol) and a low amount of protein (8.6% wt/vol) has a refractive index of 1.371 RIU.<sup>34</sup> In addition, the morphology of bacteria will also affect their refractive index such as the bacillus family, which is capable of producing endospores and undergoing sporulation. The effective refractive indices of various bacillus bacteria in their vegetative and sporulation forms were measured by using immersion refractometry. The results showed that bacillus spores (1.517–1.539 RIU) have a relatively higher effective refractive index than their vegetative forms (1.387–1.400 RIU).<sup>35</sup> This is because the solid content in the spore is significantly increased from approximately 30 to 99 g per 100 ml while the water content is reduced from approximately 77.5 to 25.5 g per 100 ml.

Due to the small size of viral particles, the refractive index measurement techniques are limited and mainly based on the suspension measurement. The average refractive index of coliphages and marine phages with a capsid size ranging from 25 to 100 nm suspended in phosphate-buffered saline buffer was measured based on light scattering.<sup>36</sup> The results showed that these viruses have a relative average refractive index of 1.025 to 1.177. Due to the limitation of the measurement technique, not much information can be studied to understand viruses based on refractive index.

Since cell refractive index is correlated with the concentration of matter, the first direct application of cell refractive index is cell growth monitoring. In the cell cycle (Fig. 2a), the cell first enters the G<sub>1</sub> phase and grows by producing proteins and cytoplasmic organelles, then enters the S phase whereby chromosomes are replicated, followed by entering the G<sub>2</sub> phase to grow more and finally divide in the M phase. Since the DNA content in the nucleus is doubled in the G<sub>2</sub>/M phases as compared to the G<sub>1</sub>/S phases, the nuclear refractive index of HeLa cells (trypsinized and resuspended in Cytolyt, solidified by HistoGel and fixed in 10% formalin) was measured and shown to increase from 1.5495 to 1.5515 RIU (Fig. 2b).<sup>37</sup> The growth of human osteosarcoma (U2OS) cells was also studied and they were transfected with YFP-proliferating cell nuclear antigen (PCNA) to monitor their progression through the S phase.<sup>38</sup> From the results, U2OS cells exhibited clear exponential growth in the G<sub>2</sub> phase and typically doubled their mass by the end of the G<sub>2</sub> phase (Fig. 2c). After mitosis, daughter cells are typically half of their parents' doubled mass. A similar observation was recorded for the growth of *E. coli*. During the growth, *E. coli* underwent

binary fission whereby DNA was replicated, its size was increased and new daughter cells were formed with the complete development of a new cell wall. The growth rate of *E. coli* was shown to be linearly proportional to the cell mass, which indicated the exponential growth behavior of *E. coli*. The nuclear division during binary fission was also observed by immersion refractometry.<sup>39</sup> The cycle started as sister nuclei were separated, forming a septum. The nucleus appeared like a 3-lobed structure. The individual lobes divided as they remained connected together. Then, the nuclear lobes moved apart, and the sister cells were completely separated at the opposite ends of the cell. This cell cycle continued for a new division for thirty minutes. On the other hand, cell-surface interaction can also be quantified by using a photonic crystal enhanced microscopy with sufficient spatial resolution to monitor the cell membrane and intra-cell attachment distribution, and temporal resolution to investigate different biological processes such as chemotaxis, apoptosis, differentiation and division.<sup>40</sup>

**Hematology.** There are several types of cells in the blood stream, which include red blood cells, white blood cells and platelets. Red blood cells are oval biconcave disks with a relatively simpler cell structure. They lack a cell nucleus and most organelles but are rich in hemoglobin. Based on tomographic bright field imaging, red blood cells have a mean refractive index of 1.402, a dry mass of 27.2 pg, a diameter of 7.0  $\mu\text{m}$ , a volume of 100.7 fL and a density of 27.1 pg fL<sup>-1</sup>.<sup>30</sup>

Similarly, the platelets that help sustain hemostatic and arterial thrombosis especially fibrillation are a subcellular fragment of blood without a cell nucleus. The two types of platelets that help separate between healthy and unhealthy

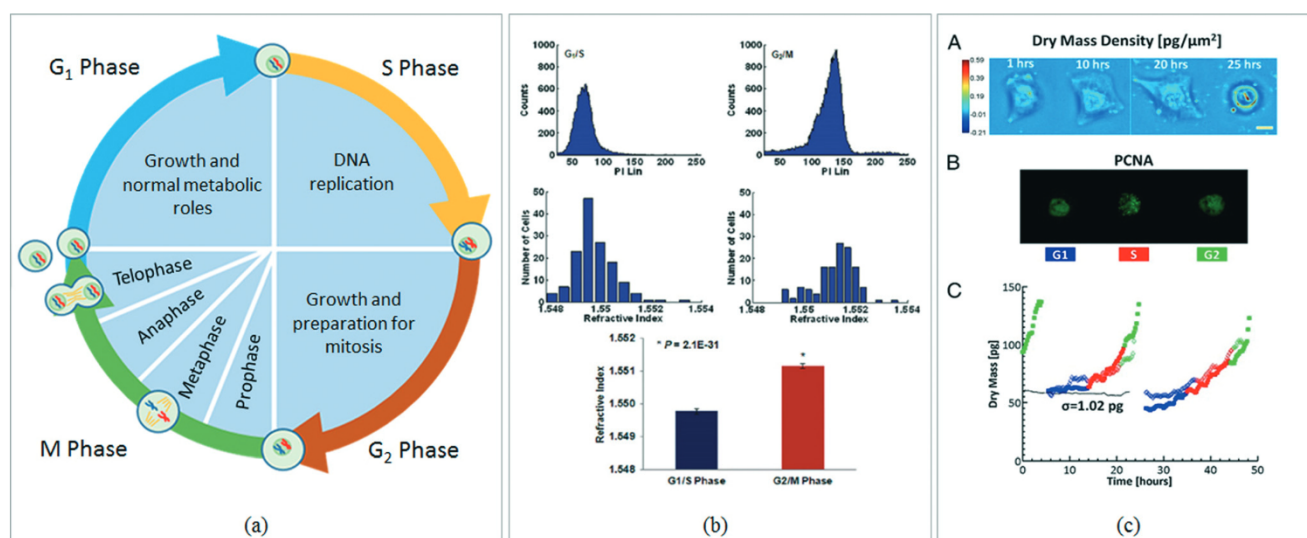


**Fig. 2** Cell cycle vs. refractive index: (a) typical cell cycle whereby the cell grows in the G<sub>1</sub> phase, DNA replicates in the S phase and the cell continues to grow in the G<sub>2</sub> phase, followed by cell division in the M phase. (b) Flow cytometry and corresponding nuclear refractive index histogram of HeLa cells arrested at the G<sub>1</sub>/S and G<sub>2</sub>/M phases, and statistical analysis of the refractive index from the cell nuclei. (Reprinted with permission from ref. 37. Copyright 2011 SPIE.) (c) U2OS growth over 2 days whereby A shows the dry mass density maps of a single U2OS cell over a cell cycle, B shows the GFP fluorescence images indicating PCNA activity, and C shows the dry mass vs. time for a cell family from 1 cell being divided to 2 and then to 4. (Reprinted with permission from ref. 38. Copyright 2011 PNAS.)



individuals with diseases are in the form of activated and inactivated platelets. In the activated state, the platelets have a spherical needle-like structure, while the inactivated state has a discoid shape with a diameter of 2–4  $\mu\text{m}$  and a thickness of 0.5–2  $\mu\text{m}$ .<sup>41</sup> During activation whereby oxygen enters into blood plasma, a temporary protrusion results in a spherical platelet cell. Due to this difference, platelets are a useful means to determine certain diseases such as cerebrovascular disease, ischemic heart disease and renovascular disease.<sup>42–44</sup> The refractive index of the platelet cell was measured to be 1.390 RIU in the range of 1.360–1.409 RIU.<sup>41,45</sup>

On the other hand, white blood cells are the body's main line of defense. There are five types of white blood cells in the blood stream, *i.e.* lymphocytes, monocytes, eosinophils, basophils, and neutrophils. Their sizes are in the range of 6–10  $\mu\text{m}$ . Lymphocytes have a relatively simpler structure with a nucleus and a small amount of cytoplasm, monocytes has a kidney-shaped nucleus, and others have a multilobed nucleus and granules in the cytoplasm as shown in Fig. 3a.<sup>46</sup> Based on light scattering and multiple-layer spherical models, lymphocytes and monocytes were measured to have a nuclear refractive index of  $1.43 \pm 0.05$  RIU and  $1.43 \pm 0.04$  RIU, respectively; and a cytoplasmic refractive index of  $1.356 \pm 0.009$  RIU and  $1.348 \pm 0.004$  RIU, respectively.<sup>47</sup> Based on immersion refractometry, lymphocytes were measured with a cytoplasmic refractive index of 1.3572 RIU,<sup>48</sup> which is lower

than the one measured by light scattering because of the effective refractive index model. Researchers showed that lymphocytes from infected or vaccine injected animals have a higher refractive index equivalent to 1% to 2% of the protein concentration due to the production of antibodies.<sup>49,50</sup>

As human red blood cells lack a nucleus and cellular organelles, by obtaining the refractive index of the cytoplasm of the red blood cells, the concentration of hemoglobin can be determined, *i.e.*  $n_{\text{rbc}} - n_0 = \beta C_{\text{hemoglobin}}$ , where  $n_0 = 1.335$  is the refractive index of cell fluid without hemoglobin and  $\beta = 0.0019 \text{ dL g}^{-1}$ .<sup>51</sup> The hemoglobin concentration for hypochromic anemia patients is relatively lower (37.9 vs. 27.4  $\text{g dL}^{-1}$ ). On the other hand, for sickle cell anemia whereby the red blood cell is distorted into a crescent shape and has a stiffer cell membrane, the stiffness of the red blood cell can be determined by dynamically measuring the fluctuation of the cell membrane using quantitative phase imaging.<sup>52</sup> Another major disease of red blood cells is malaria with 250 million people infected yearly. Hence, it is crucial to detect malaria more effectively, allowing early treatment and reducing fatality. Malaria is caused by a protozoan parasite, transmitted by mosquitoes that invade liver cells and red blood cells. Four species of *plasmodium* can infect humans and cause malaria, *i.e.* *Plasmodium falciparum* (*P. falciparum*), *P. vivax*, *P. malariae* and *P. oval*. However, not all the species are fatal in which only *P. falciparum* caused malaria leads to lethal

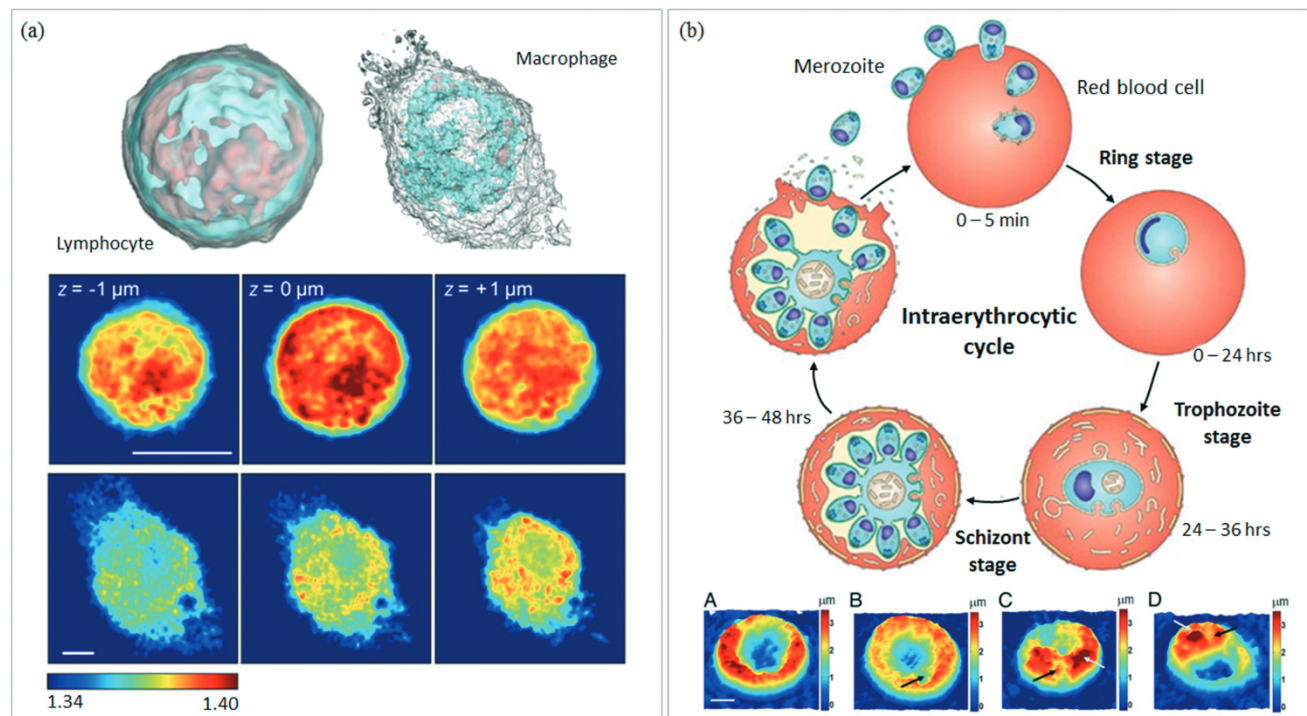


**Fig. 3** Applications of cell refractive index in hematology. (a) Rendered iso-surfaces of the refractive index map of a lymphocyte and a macrophage from the cross-sectional images of 3D refractive index tomograms in various axial planes. (Reprinted with permission from ref. 46. Copyright 2015 OSA Publishing.) (b) Schematic illustration of the intraerythrocytic cycle of malaria infection (Reprinted with permission from ref. 53. Copyright 2006 Nature.) and its 3D phase mapping at various stages (A: healthy cell, B: ring stage, C: trophozoite stage, and D: schizont stage) with black arrows indicating the merozoite and gray arrows indicating the hemozoin. (Reprinted with permission from ref. 55. Copyright 2008 PNAS.)

infection and results in most deaths, while *P. vivax* leads to severe disability after infection. The malaria infection cycle starts when mosquitoes feed on people. As the mosquitoes feed on human blood, malaria parasites called sporozoites are injected into human tissues. The sporozoites travel to the blood stream and invade the liver cells, which are called hepatocytes. As the hepatocytes burst, the parasites are released into the bloodstream as merozoites to attack the red blood cells and start an intraerythrocytic cycle as shown in Fig. 3b.<sup>53</sup> The intraerythrocytic cycle causes structural, biochemical and mechanical changes to the red blood cells. The cycle starts from the ring stage at which the merozoites invade the red blood cells and become uni-nucleated trophozoites. At the schizont stage, trophozoites develop into multi-nuclei cells called schizonts. The growth of the schizonts is based on the digestion of hemoglobin with the production of hemozoin.<sup>54</sup> These schizonts undergo differentiation to form multiple merozoite cells in the red blood cells, and the discocyte shape of the red blood cell is lost during progression to the schizont stage. Tomographic phase microscopy is used to determine the refractive index change in the red blood cells after *P. falciparum* infection through all the different stages; from healthy red blood cells to the ring stage, trophozoite and schizont stage.<sup>55</sup> Healthy red blood cells have a homogeneous distribution in refractive index, while infected red blood cells show non-homogeneous refractive index throughout the cytoplasm of the cell. The lack of homogeneity in the infected blood cells may be due to several different factors, such as hemoglobin is metabolized and transformed into a hemozoin crystal in the *P. falciparum* membrane. The vacuole of parasite occupies part of the cytoplasm of the red blood cells and several types of parasite proteins are transferred from the parasite into the cytoplasm of the infected red blood cells. Parasites cause changes to both the internal and membrane structures of the red blood cells. There is a significant refractive index difference between the healthy and the infected red blood cells. The healthy red blood cells have refractive index of  $1.399 \pm 0.006$  RIU, whereas the infected red blood cells have a refractive index of  $1.395 \pm 0.005$  RIU in the ring stage,  $1.383 \pm 0.005$  RIU in the trophozoite stage, and finally  $1.373 \pm 0.006$  RIU in the schizont stage.<sup>55</sup> This indicates a significant decreasing trend in the refractive index of the red blood cells during the infection process. The decrement of refractive index of the infected red blood cells is correlated with the decrease in the hemoglobin concentration. As the infection proceeds, the cytoplasm volume decreases as compared to the healthy red blood cells. As a result, the red blood cell's refractive index and morphology can be used as important parameters for disease diagnosis such as malaria and anemia. In addition, the refractive index of various cells in blood sample can be further studied and developed as one of the indicators in hematology laboratory diagnosis.

**Pathology.** Certain abnormalities identified in cancer cells are increased nuclear size, irregular shape and uneven chromatin texture.<sup>56</sup> Based on these characteristics along with the advancements in nanoscale detection techniques, prognosis

and early detection is becoming a real possibility. Various research studies have characterized the refractive index of normal and cancer cells, aiming to better understand the abnormal cell cycles and increased proliferation of the cancer cells. Most normal cells have a refractive index of 1.353 RIU and cancer cells have a higher refractive index ranging from 1.370 to 1.400 RIU.<sup>14,57</sup> As many human cancer cells show atypical cell cycles and increase in cell proliferation, the increase in the refractive index may be related to the increase in cell production during various stages of cell cycle in cancer patients. Specimens of breast biopsies were studied by measuring the cell refractive index using spatial-domain low-coherence quantitative phase microscopy.<sup>58</sup> Three groups of cells were measured, *i.e.* normal cells, uninvolved cells (cancer cells that are diagnosed as normal cells) and malignant cells. The results showed that the nuclear refractive index is increased from 1.542, 1.544 to 1.545 RIU, suggesting that the nuclear refractive index may be an important parameter for early-stage cancer diagnosis. Clinical studies show that circulating tumor cells (CTCs) are present in the blood stream when cancer metastasis occurs. The concentration of CTCs in the blood stream is critical and correlated with the overall survival rate of cancer such as breast, prostate and colorectal. However, the concentration of CTCs (10 per ml) is relatively very low as compared to white blood cells ( $10^6$  per ml) and red blood cells ( $10^9$  per ml), which significantly increases the difficulties in detecting CTCs. The biophysical properties of CTCs and leukocytes in an ovarian cancer patient were measured and compared by using quantitative phase imaging.<sup>59</sup> The results showed that CTCs have a higher mass (33.6 *vs.* 18.7 pg), a greater volume (518.2 *vs.* 230.0 fL) and a lower dry mass density (0.065 *vs.* 0.085 pg fL<sup>-1</sup>) as compared to leukocytes (Fig. 4a). These results provide insight into the development of a label-free biophysical CTC detection system, and aid in understanding the genetic and proteomic composition of CTCs for targeted therapies.

Prevention of parasite infection through detection of bacteria and virus in water and food has been an ongoing process with vast improvements over the years due to new technologies that reduce the amount of detection time and costs. The current standard method used for bacteria detection in drinking water is the USEPA Method 1604.<sup>60</sup> Several technological limitations exist in this method that impede its effectiveness in preventing a bacteria outbreak, such as laboratory-based and long processing time. Hence, much effort is made to reduce the amount of detection time and find a more cost effective on-site method. Several potential methods have come up and one of them is using the refractive index and morphology of different bacteria to correctly identify the source of an infection.<sup>61</sup> An on-chip optofluidic refractometry<sup>12</sup> that can detect the refractive index and morphology of a single bacterium in real-time was demonstrated for the characterization of three different bacteria species, *i.e.* *E. coli*, *Shigella flexneri* and *Vibrio cholerae* (Fig. 4b). The results showed that the three bacteria have distinctive refractive index values, demonstrating the



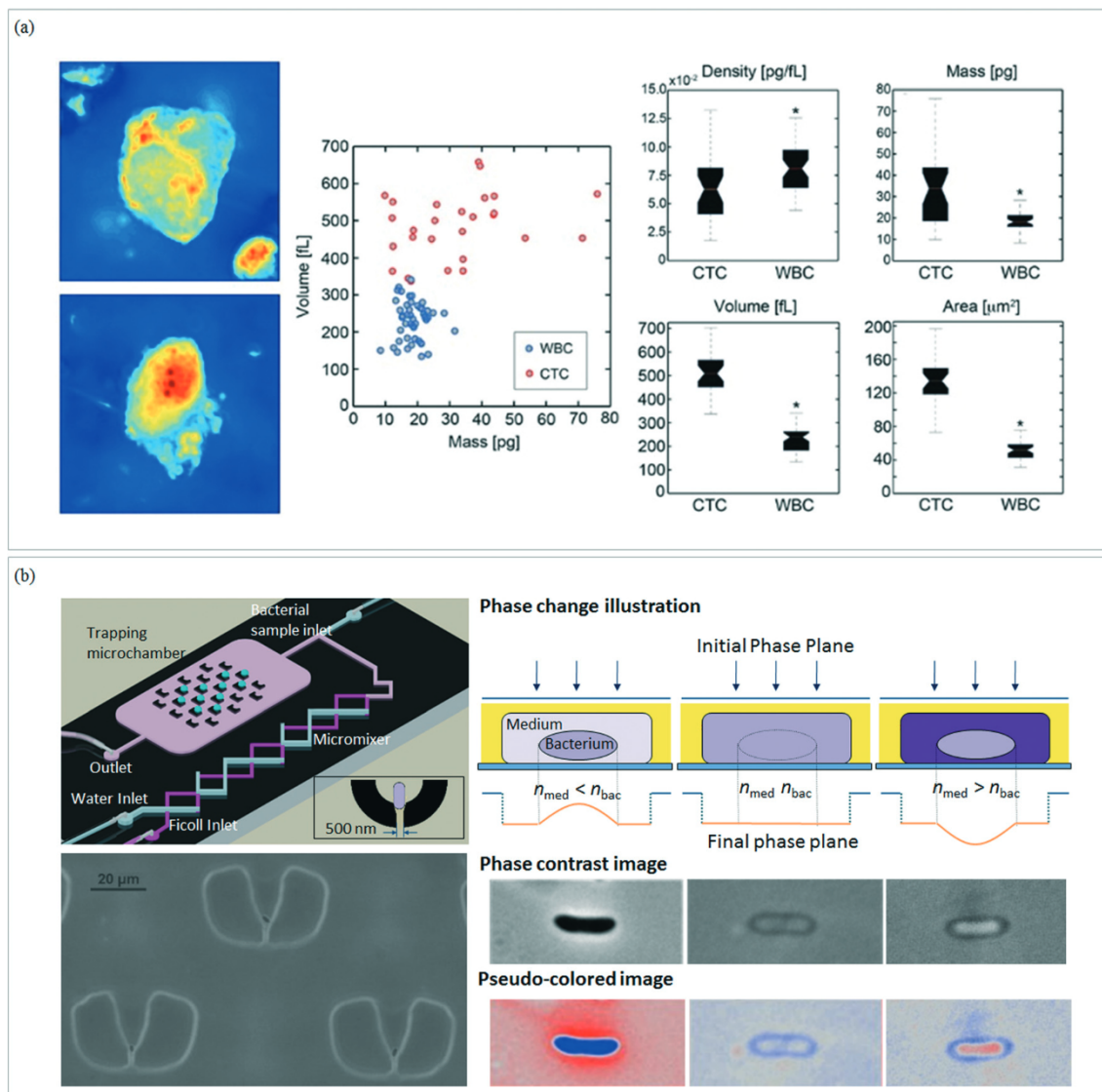


**Fig. 4** (a) Quantitative phase microscopy of circulating tumor cells (CK + CD45-DAPI + HD-CTC5 and the statistical analysis of density, mass, volume and area comparison between white blood cells and CTCs. (Reprinted with permission from ref. 59. Copyright 2012 Frontiers.) (b) Optofluidic immersion refractometer for measuring the effective refractive index of single bacterium by varying the external medium to match that of the bacterium. (Reprinted with permission from ref. 12. Copyright 2014 RSC Publishing.)

potential applications of using refractive index for bacteria identification by building a morphology and refractive index database.

Quantitative phase microscopy was also used to monitor the refractive index change in infected host cells such as *Salmonella*-infected bone marrow derived macrophages.<sup>62</sup> In one study, the dynamic cell morphological changes in rat basophilic leukemia RBL-2H3 cells infected with *Vibrio vulnificus* strains were investigated.<sup>63</sup> The results showed that infected RBL-2H3 cells increased gradually after infection due to the influx of water through micropores formed on the membrane affected by the infection. Typically, around 76 min after infection, the cell volume showed an unrecoverable sharp decline, which is presumably due to the irreversible cell death process.

## Outlook for cell refractive index

Cell refractive index is a fundamental biophysical parameter that correlated with the intracellular contents, cell size, mass, etc. It is critical to consider the following criteria when cell refractive index is used for cell analysis and disease diagnosis:

(1) *Statistical sample size* – cell refractive index, size, mass, etc. vary in range even for the same cell species. In such a case, it may not be conclusive to determine cell types or states with a limited number of cells. To extract meaningful and correlated information from the cell refractive index, it is essential to have a sufficiently large number of cells.

(2) *Non-specificity* – unlike other label-free techniques such as coherent anti-Stoke Raman scattering, cell refractive index is non-specific to chemical or protein molecules. However, it

has huge potential in complement to existing biochemical techniques such as fluorescence biomarkers to provide more complete information on the target specimens. Most techniques for the measurement of cell refractive index are compatible and can be easily integrated with fluorescence detection. With specificity provided by fluorescence biomarkers, more in-depth analysis of cell refractive index in cell biology and disease diagnosis can be performed.

(3) *Dependent on measurement conditions* – the measurement of cell refractive index greatly depends on the chemical pre-treatments and extracellular conditions such as live or fixed samples, chemical treatments, temperature, osmotic pressure, culture medium, etc. For example, the nuclear refractive index of live and fixed HeLa cells was measured with values of 1.355–1.365 (ref. 28) and 1.550–1.552,<sup>37</sup> respectively. Therefore, for any investigation to correlate cell refractive index with cell state or disease diagnosis, experimental conditions have to be controlled and maintained throughout the experiments.

(4) *Lateral resolution* – previously, only the average refractive index of suspended cells or the effective refractive index of a single cell can be measured, which limits the applications of cell refractive index due to the lack of details and resolution. With the advanced development of optical imaging techniques, cell refractive index mapping offers substantial resolution and detailed information for the studies of cell biology, hematology and pathology. Not only diffraction limited lateral resolution is preserved, but rapid temporal resolution and 3D live cell imaging can also be realized. However, the diffraction limit of lateral resolution may hinder the applications of cell refractometry for nano-sized viral particles in virological studies or single molecule or sub-cellular organelle analysis. Similar to super-resolution fluorescence imaging techniques, which can image labelled samples beyond the diffraction limit to several tenths of nanometer, phase nanoscopy is the future trend of cell refractometry for technological and scientific breakthrough. Indeed, time-lapse phase nanoscopy with a lateral phase resolution of 90 nm is developed,<sup>64</sup> which uses a nanoscale aperture with a diameter of 75 nm to improve the light quality, leading to improved lateral resolution.

On the other hand, robust and high throughput manipulation methods for cells and liquids in microfluidic platforms have gained more attention in the research community of cell refractometry. Microfluidics is employed not only to deliver a single cell into resonant cavities for effective cell refractive index measurements, but also to control the flow of cells, passing through the sample beam of quantitative phase imaging, and generate a time sequence of interference images for 3D refractive index mapping.<sup>29</sup> The integration of advanced optical imaging techniques into the microfluidic platform can also facilitate the dynamic studies of cultured cells. Applications such as localized chemical or optical stimulation of patterned neuron networks in a microfluidic chip,<sup>65,66</sup> the mechanical motions of cancer cells through structural barriers,<sup>67</sup> the effect of cells under constant and pulsatile

shear stresses and chemical stimulants<sup>68,69</sup> are among the important biomedical research areas of microfluidics. By combining with advanced optical imaging techniques to measure and monitor the refractive index distribution of cells, new biological insight will be obtained since localized changes down to 100 nm can be easily measured. One specific interesting area is the application of cell refractive index in flow cytometry. Current flow cytometry only uses scattering signals as a parameter for gating without providing much information on the sample. With the advanced development in cell refractive index measurement techniques, in the future, cell refractive index and size can replace scattering signals to provide direct information on the tested sample in complement to fluorescence signals. Another application will be long-period cell monitoring in the microfluidic platform for disease diagnosis. For example, the changes in host cell morphology and intracellular organelles can be monitored and studied by using 2D refractive index mapping in high spatio-temporal resolutions during virus infection to investigate the infection cycle, aiming to develop a rapid virus infectivity technique.

## Conclusions

Cell refractive index is one of the key biophysical parameters extensively studied starting from the average refractive index of suspended cells and the effective refractive index of a single cell to the recent 2D and 3D refractive indices of a single cell. With the development of advanced optical imaging techniques to measure cell refractive index with an ultra-high spatial resolution (100 nm), various new biological insights are provided by studying cell refractive index, such as cell morphology and growth in cell biology, malaria and anemia disease diagnosis in hematology, and cancer cell and circulating tumor cell detection in pathology. The synergy between microfluidics and cell refractometry has pushed such cutting-edge research to high-throughput and high-controllability cell dynamics monitoring using optical imaging techniques with high temporal, spatial and axial resolutions. The continuous efforts to improve its spatial and axial resolutions and extending its applications to water and environmental monitoring, food safety monitoring, other biomedical and biological areas such as virology and single molecule analysis will be the main future trends.

## Acknowledgements

This work was supported by the Singapore National Research Foundation under its Environmental & Water Technologies Strategic Research Programme (1102-IRIS-05-01/02/04/05), which is administered by the Environment & Water Industry Programme Office (EWI) of the PUB.

## References

- 1 G. Bao and S. Suresh, *Nat. Mater.*, 2003, 2, 715–725.
- 2 E. S. Boyden, F. Zhang, E. Bamberg, G. Nagel and K. Deisseroth, *Nat. Neurosci.*, 2005, 8, 1263–1268.



- 3 F. D. Bryant, B. A. Seiber and P. Latimer, *Arch. Biochem. Biophys.*, 1969, **135**, 79–108.
- 4 A. H. Hielscher, J. R. Maurant and I. J. Bigio, *Appl. Opt.*, 1997, **36**, 125–135.
- 5 J. B. Bateman, J. Wagman and E. L. Carstensen, *Colloid Polym Sci.*, 1966, **208**, 44–58.
- 6 A. E. Balaev, K. N. Dvoretzki and V. A. Doubrovski, *Proc. SPIE*, 2002, **4707**, 253–260.
- 7 P. S. Tuminello, E. T. Arakawa, B. N. Khare, J. M. Wrobel, M. R. Querry and M. E. Milham, *Appl. Opt.*, 1997, **36**, 2818–2824.
- 8 R. Barer, *J. Opt. Soc. Am.*, 1957, **47**, 545–556.
- 9 R. Barer, K. F. A. Ross and S. Tkaczyk, *Nature*, 1953, **171**, 720–724.
- 10 R. Barer and S. Joseph, *Q. J. Microsc. Sci.*, 1954, **95**, 399–423.
- 11 S. Joseph, *J. Microsc.*, 1983, **131**, 163–172.
- 12 P. Y. Liu, L. K. Chin, W. Ser, T. C. Ayi, P. H. Yap, T. Bourouina and Y. Leprince-Wang, *Lab Chip*, 2014, **14**, 4237–4243.
- 13 R. A. Flynn, B. Shao, M. Chachisvilis, M. Qzkan and S. C. Esener, *Biomed. Microdevices*, 2005, **7**, 93–97.
- 14 X. J. Liang, A. Q. Liu, C. S. Lim, T. C. Ayi and P. H. Yap, *Sens. Actuators, A*, 2007, **133**, 349–354.
- 15 W. Z. Song, X. M. Zhang, A. Q. Liu, C. S. Lim, P. H. Yap and H. M. M. Hosseini, *Appl. Phys. Lett.*, 2006, **89**, 203901.
- 16 L. K. Chin, A. Q. Liu, X. M. Zhang, C. S. Lim, J. H. Ng, J. Z. Hao and S. Takahashi, *Appl. Phys. Lett.*, 2007, **91**, 243901.
- 17 W. Z. Song, A. Q. Liu, S. Swaminathan, C. S. Lim, P. H. Yap and T. C. Ayi, *Appl. Phys. Lett.*, 2007, **91**, 223902.
- 18 K. J. Moh, X. C. Yuan, J. Bu, S. W. Zhu and B. Z. Gao, *Opt. Express*, 2008, **16**, 20734–20740.
- 19 J. Lee, C. Lee, E. Lin and P. Wei, *Appl. Phys. Lett.*, 2008, **93**, 173110.
- 20 C. L. Curl, C. J. Bellair, T. Harris, B. E. Allman, P. J. Harris, A. G. Stewart, A. Roberts, K. A. Nugent and L. M. Delbridge, *Cytometry, Part A*, 2005, **65**, 88–92.
- 21 F. Charrière, A. Marian, F. Montfort, J. Kuehn, T. Colomb, E. Cuche, P. Marquet and C. Depeursinge, *Opt. Lett.*, 2006, **31**, 178–180.
- 22 B. Rappaz, P. Marquet, E. Cuche, Y. Emery, C. Depeursinge and P. J. Magistretti, *Opt. Express*, 2005, **13**, 9361–9373.
- 23 N. Lue, W. Choi, G. Popescu, Z. Yaqoob, K. Badizadegan, R. R. Dasari and M. S. Feld, *J. Phys. Chem. A*, 2009, **113**, 13327–13330.
- 24 J.-W. Su, W.-C. Hsu, C.-Y. Chou, C.-H. Chang and K.-B. Sung, *J. Biophotonics*, 2013, **6**, 416–424.
- 25 Y.-C. Chua, W.-Y. Chang, K.-H. Chen, J.-H. Chen, B.-C. Tsai and K. Y. Hsu, *Optik*, 2014, **125**, 3307–3310.
- 26 W.-C. Hsu, J.-W. Su, T.-Y. Tseng and K.-B. Sung, *Opt. Lett.*, 2014, **39**, 2210–2213.
- 27 N. M. Dragomir, X. M. Goh and A. Roberts, *Microsc. Res. Tech.*, 2008, **1**, 5–10.
- 28 W. Choi, C. Fang-Yen, K. Badizadegan, S. Oh, N. Lue, R. R. Dasari and M. S. Feld, *Nat. Methods*, 2007, **4**, 717–719.
- 29 Y. Sung, N. Lue, B. Hamza, J. Martel, D. Irimia, R. R. Dasari, W. Choi, Z. Yaqoob and P. So, *Phys. Rev. Appl.*, 2014, **1**, 014002.
- 30 K. G. Phillips, S. L. Jacques and O. J. T. McCarty, *Phys. Rev. Lett.*, 2012, **109**, 118105.
- 31 K. Haseda, K. Kanematsu, K. Noguchi, H. Saito, N. Umeda and Y. Ohta, *Biomed. Opt. Express*, 2015, **6**, 859–869.
- 32 J. D. Wilson, W. J. Cottrell and T. H. Foster, *J. Biomed. Opt.*, 2007, **12**, 014010.
- 33 A. Brunsting and P. F. Mullaney, *Biophys. J.*, 1974, **14**, 439–453.
- 34 J. A. Valkenburg and C. L. Woldringh, *J. Bacteriol.*, 1984, **160**, 1151–1157.
- 35 K. F. A. Ross and E. Billing, *J. Gen. Microbiol.*, 1957, **16**, 418–425.
- 36 W. M. Balch, J. Vaughn, J. Novotny, D. T. Drapeau, R. Vaillancourt, J. Lapierre and A. Ashe, *Limnol. Oceanogr.*, 2000, **45**, 492–498.
- 37 R. K. Bista, S. Uttam, P. Wang, K. Staton, S. Choi, C. J. Bakkenist, D. J. Hartman, R. E. Brand and Y. Liu, *J. Biomed. Opt.*, 2011, **16**, 070503.
- 38 M. Mira, Z. Wang, Z. Shen, M. Bednarz, R. Bashira, I. Golding, S. G. Prasant and G. Popescu, *Proc. Natl. Acad. Sci. U. S. A.*, 2011, **108**, 13124–13129.
- 39 D. J. Mason and D. M. Powelson, *J. Bacteriol.*, 1956, **71**, 474–479.
- 40 W. Chen, K. D. Long, M. Lu, V. Chaudhery, H. Yu, J. S. Choi, J. Polans, Y. Zhuo, B. A. C. Harley and B. T. Cunningham, *Analyst*, 2013, **138**, 5886–5894.
- 41 I. V. Kolesnikova, S. V. Potapov, M. A. Yurkin, A. G. Hoekstra, V. P. Maltsev and K. A. Semyanov, *J. Quant. Spectrosc. Radiat. Transfer*, 2006, **102**, 37–45.
- 42 D. D. McManus and J. E. Freedman, *Nat. Rev. Cardiol.*, 2015, **12**, 711–717.
- 43 L. Vizioli, S. Muscari and A. Muscari, *Int. J. Clin. Pract.*, 2009, **2063**, 1509–1515.
- 44 J. T. Daugirdas and A. A. Bernardo, *Kidney Int.*, 2012, **82**, 147–157.
- 45 A. E. Moskalensky, M. A. Yurkin, A. I. Konokhova, D. I. Strokotov, V. M. Nekrasov, A. V. Chernyshev, G. A. Tsvetovskaya, E. D. Chikova and V. P. Maltsev, *J. Biomed. Opt.*, 2013, **18**, 017001.
- 46 J. Yoon, K. Kim, H. Park, C. Choi, S. Jang and Y. Park, *Biomed. Opt. Express*, 2015, **6**, 3865–3875.
- 47 V. P. Maltsev, A. G. Hoekstra and M. A. Yurkin, *Optics of White Blood Cells: Optical Models, Simulations, and Experiments, in Advanced Optical Flow Cytometry: Methods and Disease Diagnoses*, ed. V. V. Tuchin, Wiley-VCH Verlag GmbH & Co. KGaA, Weinheim, Germany, 2011.
- 48 K. W. Keohane and W. K. Metcalf, *Q. J. Exp. Physiol. Cogn. Med. Sci.*, 1959, **44**, 343–350.
- 49 J. G. Wilde and W. K. Metcalf, *Ann. Clin. Lab. Sci.*, 1975, **5**, 23–26.
- 50 K. W. Keohane and W. K. Metcalf, *Nature*, 1959, **183**, 4655.
- 51 N. Ghosh, P. Buddhiwant, A. Uppal, S. K. Majumder, H. S. Patel and P. K. Gupta, *Appl. Phys. Lett.*, 2006, **88**, 084101.
- 52 N. T. Shaked, L. L. Satterwhite, M. J. Telen, G. A. Truskey and A. Wax, *J. Biomed. Opt.*, 2011, **16**, 030506.
- 53 K. Haldar, S. Kamoun, N. L. Hiller, S. Bhattacharje and C. van Ooij, *Nat. Rev. Microbiol.*, 2006, **4**, 922–931.

- 54 I. Weissbuch and L. Leiserowitz, *Chem. Rev.*, 2008, **108**, 4899–4914.
- 55 Y. Park, M. Diez-Silva, G. Popescu, G. Lykotrafitis, W. Choi, M. S. Feld and S. Suresh, *Proc. Natl. Acad. Sci. U. S. A.*, 2008, **105**, 13730–13735.
- 56 S. Suresh, *Acta Mater.*, 2007, **55**, 3989–4014.
- 57 W. J. Choi, D. I. Jeon, S.-G. Ahn, J.-H. Yoon, S. Kim and B. H. Lee, *Opt. Express*, 2010, **18**, 23285–23295.
- 58 P. Wang, R. Bista, R. Bhargava, R. E. Brand and Y. Liu, *Opt. Lett.*, 2010, **35**, 2840–2842.
- 59 K. G. Phillips, C. RuizVelasco, J. Li, A. Kolatkar, M. Lutten, K. Bethel, B. Duggan, P. Kuhn and O. J. T. McCarty, *Front. Oncol.*, 2012, **2**, 1–8.
- 60 J. Olstadt, J. J. Schauer, J. Standridge and S. Kluender, *J. Water Health*, 2007, **5**, 267–282.
- 61 Y. Jo, J. Jung, J. W. Lee, D. Shin, H. Park, K. T. Nam, J.-H. Park and Y. Park, *Sci. Rep.*, 2014, **4**, 5090.
- 62 A. E. Ekpenyong, S. M. Man, S. Achouri, C. E. Bryant, J. Guck and K. J. Chalut, *J. Biophotonics*, 2013, **6**, 393–397.
- 63 S. Lee, Y. R. Kim, J. Y. Lee, J. H. Rhee, C. S. Park and D. Y. Kim, *J. Biomed. Opt.*, 2011, **16**, 036004.
- 64 Y. Cotte, F. Toy, P. Jourdain, N. Pavillon, D. Boss, P. Magistretti, P. Marquet and C. Depeursinge, *Nat. Photonics*, 2013, **7**, 113–117.
- 65 J. El-Ali, P. K. Sorger and K. F. Jensen, *Nature*, 2006, **442**, 403–411.
- 66 L. J. Millet, M. E. Stewart, R. G. Nuzzo and M. U. Gillette, *Lab Chip*, 2007, **10**, 1525–1535.
- 67 Y. Fu, L. K. Chin, T. Bourouina, A. Q. Liu and A. M. J. VanDongen, *Lab Chip*, 2012, **12**, 3774–3778.
- 68 L. K. Chin, J. Q. Yu, Y. Fu, T. Yu, A. Q. Liu and K. Q. Luo, *Lab Chip*, 2011, **11**, 1856–1863.
- 69 J. Q. Yu, X. F. Liu, L. K. Chin, A. Q. Liu and K. Q. Luo, *Lab Chip*, 2013, **13**, 2693–2700.